



This is a repository copy of *Ultrafast synthesis of 13X@NaA composites through plasma treatment for highly selective carbon capture.*

White Rose Research Online URL for this paper:
<http://eprints.whiterose.ac.uk/122046/>

Version: Accepted Version

Article:

Huang, J., Hu, J., Du, W. et al. (3 more authors) (2017) Ultrafast synthesis of 13X@NaA composites through plasma treatment for highly selective carbon capture. *Journal of Materials Chemistry A*, 35. pp. 18801-18807. ISSN 2050-7488

<https://doi.org/10.1039/c7ta05649d>

Reuse

Items deposited in White Rose Research Online are protected by copyright, with all rights reserved unless indicated otherwise. They may be downloaded and/or printed for private study, or other acts as permitted by national copyright laws. The publisher or other rights holders may allow further reproduction and re-use of the full text version. This is indicated by the licence information on the White Rose Research Online record for the item.

Takedown

If you consider content in White Rose Research Online to be in breach of UK law, please notify us by emailing eprints@whiterose.ac.uk including the URL of the record and the reason for the withdrawal request.



eprints@whiterose.ac.uk
<https://eprints.whiterose.ac.uk/>



An ultra-fast synthesis of 13X@NaA composites through the plasma treatment for high selective carbon capture

Jiali Huang,^a Jun Hu*^a, Wenli Du^b, Honglai Liu^a, Feng Qian^b, Meilong Wang*^c,

Received 00th January 20xx,
Accepted 00th January 20xx

DOI: 10.1039/x0xx00000x

www.rsc.org/

The primary challenge in material design and fabrication is achieving excellent performance, economical substances, fast and convenient synthesis for real world applications. We tackle this challenge by an ultra-fast synthesis of core-shell 13X@NaA zeolite composites within only 30 min. By using the plasma treatment, more silanol groups on the surface of 13X powders and hydroxyl radicals in NaA precursor gel result in the accelerated formation of NaA crystal shell. After the potassium ion exchange in different degrees, the obtained 13X@NaA composites exhibit extremely high selectivity of CO₂ over N₂ of 149~380 and maintain good capacity of 3.41~1.84 mmol·g⁻¹. Our work provides a promising approach for synthesis of core-shell zeolite composites as economic materials for further multiple applications.

Introduction

Carbon capture is not optional if the world hopes to limit future temperature increases. Currently, the adsorption technology is one of promising approaches for CO₂ capture, in which zeolites are the most practicable commercial adsorbents.^{1,2} However, their low selectivity of CO₂ over other gases such as N₂ and H₂O becomes a bottleneck of the wide applications in reality. Zeolite composites have spurred great research interest since they can combine unique properties of the each component zeolite simultaneously.^{3,4} We can anticipate zeolite composites with the core-shell structure by carefully designing the shell [structure could significantly improve CO₂ selectivity, and preserve the good adsorption capacity of the core zeolites, simultaneously](#). However, the common nucleation and crystal growth of the core-shell zeolite composites are usually time-consuming, [such as 48 h or more](#), and difficult to control.⁵⁻⁷ Even worse, the crystal structure of core zeolites might collapse in the concentrated basic medium during the long-time and high-temperature crystallization of zeolite shell.⁸ Understanding the crystallization mechanism and increasing the formation rate of zeolites are still great challenges for the successful formation of core-shell zeolite composites.⁹⁻¹¹

The hydroxyl group presented at the surface of the core zeolite is crucial for the formation of the shell zeolite. Some physical or chemical methods, such as microwave waves¹² and sonochemical method¹³ have been used to increase the amount of active hydroxyl groups. Meanwhile, free radicals produced in the precursor solutions of the shell zeolite can also effectively accelerate its crystallization rate. Very recently, Yu's group demonstrated that the nucleation process of zeolites, such as NaA, NaX and silicalite-1, can be successfully accelerated by introducing hydroxyl free radicals ($\cdot\text{OH}$) through the ultraviolet (UV) irradiation or Fenton's reagent.¹⁴ Among various activation methods, the plasma technology can produce energetic electrons and activated radicals^{15,16} to realize rapid and uniform surface modification.^{17,18} As a non-thermal gas discharge plasma technology, the dielectric-barrier discharge (DBD) is of the most successful method. Currently the plasma treatment is mostly applied for polymer materials,^{19,20} only a few studies explored its applications for zeolite-type molecular sieves.^{21,22} We previously developed a convenient DBD plasma treatment method to modify the internal surface of the mesoporous silica, such as SBA-15 and MCF^{23,24}. By this method, the amount of surface silanol groups were increased, accordingly, the surface grafting rate of amine was significantly accelerated, with the reaction time shortened from general 18 h to 2 h. In fact, the plasma-induced radicals not only can produce new functional groups on the material surface, but also can generate free radicals in reactant solution. Acting as the reaction active sites, those functional groups and free radicals can effectively accelerate the solid-liquid interfacial reactions.^{25,26} So far, [very few works about using the plasma treatment for core zeolite powder and \(or\) shell zeolite precursor solution have been reported, although it is anticipated the formation rate of the core-shell zeolite composites would be significantly accelerated](#).

Herein, we applied the DBD plasma method to accelerate the synthesis of core-shell zeolite composite, in which 13X zeolite

^a Key Laboratory for Advanced Materials, School of Chemistry and Molecular Engineering, East China University of Science and Technology, 130 Meilong Road, Shanghai 200237, China. E-mail: junhu@ecust.edu.cn; Tel: +86 21 64252630.

^b School of Information Science and Engineering, East China University of Science and Technology, 130 Meilong Road, Shanghai 200237, China.

^c Department of Chemical and Biological Engineering, University of Sheffield, Sir Robert Hatfield Building, Mappin Street, Sheffield S1 3JD, UK. E-mail: Meihong.Wang@sheffield.ac.uk; Tel: +44 (0) 114 222 7160.

[†] Electronic Supplementary Information (ESI) available: [XRD patterns, SEM images, TG curves, N₂ sorption isotherms, CO₂/N₂ adsorption isotherms. See DOI: 10.1039/b000000x/

(framework type code FAU) powders were chosen as the core and NaA zeolite (framework type code LTA) as the shell. 13X powders or the mixture of NaA precursor gel and 13X powders were treated under oxygen plasma, and the limitation of the crystallization time for the formation of uniform NaA shell was determined. The accelerating mechanism of the plasma treatments was illustrated by detecting the produced silanol groups and the hydroxyl radicals. After formation a thin shell of NaA on 13X core, the window size of NaA was adjusted by the potassium ion exchange. **By significantly shortening the crystallization time to only 30 min and with the degree of 18% potassium ion exchange, the thickness of NaA shell and the pore sized of the resultant 13X@NaKA composites were rationally controlled, in turn, high selectivity, high adsorption capacity and high rate for CO₂ adsorption were simultaneously obtained.** This approach demonstrated a promising way for synthesis of core-shell zeolite composites for the specific task application.

Experimental

Materials

13X zeolite powders and Methylene blue (MB) were purchased from Shanghai Jiuzhou Chemicals Co., Ltd. Sodium hydroxide (NaOH) and Sodium silicate (NaSiO₃·9H₂O) were purchased from Shanghai Lingfeng Chemicals Co., Ltd. Sodium aluminate (NaAlO₂) was purchased from Taitan Chemicals Co., Ltd.

Synthesis of core-shell 13X@NaA composites

Without the plasma treatment 13X powders were activated by heating at 500 °C for 2 h before usage. Based on the common crystallization method, 13X@NaA composites were synthesized for comparison. Typically, 1 g activated 13X powders were dispersed into a certain amount of NaA precursor gels (1.9NaOH/1.5NaAlO₂/3.5NaSiO₃·9H₂O/43H₂O). After stirring for 30 min at 333 K, the mixture slurry was transferred into an autoclave and aged at 373 K for specific time. Thereafter the sample was filtered, washed with distilled water and dried at 383 K. The obtained solid powders were denoted as 13X@NaA-N-*t*. (N means without the plasma treatment; *t* is the aging time, *t*=15, 30, 60, 120 min, respectively.)

With the plasma treatment The synthesis process and the ratio of precursor mixture of NaA gel were the same as above, except the plasma treatments were applied for the 13X powders and the precursor mixture respectively before the synthesis.

We adopted dielectric barrier discharge (DBD) method under the oxygen flow at room temperature and normal pressure (Scheme S1). Typically, 1 g activated 13X powders were added in the quartz reaction chamber and treated by DBD plasma for 10 min with different input powers, which were denoted as 13X-P-*n* (P means the plasma treatment for 13X powders; *n* is the input power, *n* = 80, 90, 100 W respectively). As shown in Scheme S2, after the plasma treatment, 13X-P-*n* powders were immediately put into NaA precursor gel to synthesize the composite. The finally resulted solid powders were denoted as 13X@NaA-P-*t*.

Alternatively, after the DBD plasma treatment for 13X powders, a certain amount of NaA precursor gels were added immediately into the quartz reaction chamber. After stirring for 30 min, the whole mixture slurry was subjected to the plasma treatment

with different input powers for 10 min again. Then, after the same synthesis, the finally obtained samples were denoted as 13X@NaA-S-*t* (S means the plasma treatment for the whole slurry).

Potassium ion exchange

As illustrated in Scheme S2, 1 g obtained 13X@NaA-S-30 or 13X@NaA-S-120 powders were added into 100 ml KCl aqueous solution (with different concentrations). After stirring for 60 min at 298 K, the sample was filtered, washed with distilled water, and dried at 383 K. The obtained powders with different degrees of potassium ion exchange were denoted as 13X@NaKA-S-*t*-*m* (*m* is the molar ratio of K⁺ to Na⁺, *m* = 8, 18, 30 %, respectively).

Characterizations

X-ray diffraction (XRD) patterns were collected on a RigakuD/MAX-2500 V/PC using Cu K α Radiation at 40 kV and 100 mA. Field-emission scanning electron microscopy (FESEM) images were taken using a Nova NanoSEM 450. The infrared spectra were carried out on a Nicolet iS10 Fourier Transform infrared spectroscopy (FTIR) with the KBr pellet technique. The ultra-violet spectrum (UV) is measured by Shimadzu, UV-2550 spectrophotometer. Nitrogen adsorption-desorption isotherms were measured at 77.4 K on a Micrometrics ASAP 2020 analyzer. The Brunauer-Emmett-Teller (BET) method was employed to calculate the specific surface areas. Thermo gravimetric (TG) analyze the quantity of functional groups by NETZSCH STA 499 F3. Inductively coupled plasma optical emission spectrometry (ICP-AES, Agilent 725ES) was employed to determine the K content in the samples with different degrees of potassium ion exchange.

Hydroxyl Radical Detection

We chose methylene blue (MB) as the trapping agent of free radicals. 5 ml 1mol·L⁻¹ NaOH was added into the quartz reaction chamber and was treated by DBD plasma under the oxygen flow for 10 min with the input power of 90 W. Then, 5 ml MB aqueous solution (with a concentration of 0.016 mmol·L⁻¹) was added immediately. The UV absorbance value *A_i* of the mixture was measured at $\lambda=664$ nm, with the deionized water as the reference. Then the apparent amount of free radicals such as hydroxyl free radical (\bullet OH) produced by the plasma treatment in the system can be calculated as Eq. 1

$$\text{Apparent yield of free radicals (\%)} = ((A_0 - A_i)/A_0) \times 100\% \quad (1)$$

where *A₀* is the absorbance value of the mixture of 5 ml MB and 5 ml NaOH without the plasma treatment.

Gas adsorption measurement

CO₂ and N₂ static adsorption capacities of the samples were determined by a Micrometrics ASAP 2020 at 298 K. All the samples were degassed for 6 h at 393 K under vacuum before the measurement. **The selectivity of CO₂ to N₂ (*S*_{CO₂/N₂}) was calculated by the ideal adsorbed solution theory (IAST) as Eq. 2,**

$$S_{\text{CO}_2/\text{N}_2} = \frac{q_1/q_2}{P_1/P_2} \quad (2)$$

where q_i is the adsorption capacity of i component at its partial pressure of p_i . Here, to simulate the flue gas (15% CO_2 , 85% N_2), we estimated $S_{\text{CO}_2/\text{N}_2}$ from the relative adsorption capacity of pure CO_2 at the pressure of 15 kPa over pure N_2 at the pressure of 85 kPa. CO_2 dynamic adsorption was tested by the thermogravimetric analysis (TGA). About 10 mg sample was placed in a flat alumina pan and it was degassed by heating to 110 °C in a pure N_2 purge about 60 min until there was no weight change. Then the temperature was decreased to 25 °C, the testing gas of the simulated flue gas (15:85 v/v of CO_2/N_2) was then introduced at a flow rate of 20 $\text{mL}\cdot\text{min}^{-1}$. After 180 min adsorption, the gas was switched into pure N_2 , and the temperature was raised again to 110 °C at a heating rate of 10 °C $\cdot\text{min}^{-1}$ to perform desorption. The flow rate of N_2 purge was set as 60 $\text{mL}\cdot\text{min}^{-1}$ to make sure all the impurities or CO_2 can be removed completely in a short time. The adsorption capacity was calculated by the sample weight change during this adsorption/desorption process.

Results and discussion

Compared the XRD patterns of 13X-P samples with that of pristine 13X (Fig. S1), the integrity of 13X structure can be maintained after the plasma treatment, therefore, the DBD plasma treatment under oxygen atmosphere can be used to improve the reaction activity without the damage of its crystal structure.

The structure evolution of 13X@NaA composites with the aging time was recorded by XRD and SEM images. After aging for 120 min (Fig. S2a), the characteristic peaks of NaA appeared in all XRD patterns of the composites samples, regardless if they were with or without the plasma treatment. But the intensity of NaA peaks in 13X@NaA-N-120 was much lower. When the aging time was shortened to 60 min (Fig. S2b), the characteristic peaks of NaA can be observed in both XRD patterns of 13X@NaA-P-60 and 13X@NaA-S-60 samples; in contrast, they disappeared in the XRD pattern of 13X@NaA-N-60 sample produced by the common crystallization method, suggesting the plasma treatment can effectively accelerate the formation rate of NaA shell. A comparative analysis of their relative crystallinity of NaA (Fig. 1b the detailed calculation method can be found in SI) revealed 13X@NaA-P-60 (41%) was weaker than 13X@NaA-S-60 (51%), thus, the double plasma treatments for both 13X powders and the mixed precursor gel can accelerate the crystallization rate more efficiently. Compared with the SEM image of octahedral-shaped of pristine 13X (Fig. S3a), the successful formation of NaA crystal shell can be clearly observed on the surface of 13X@NaA-S-60 (Fig. S3b). However, without the plasma treatment, there were only some amorphous particles formed on the surface of 13X@NaA-N-60 (Fig. S3c), consistent with its XRD result. When the aging time was further shortened to 30 min, the characteristic peaks of NaA still existed in both XRD patterns of 13X@NaA-P-30 and 13X@NaA-S-30 (Fig. 1a), but the relative crystallinity of NaA were lower (Fig. 1b). Confirmed by the SEM images (Fig. 2c), the whole particle size increased from pristine 13X of 3.5 μm to about 4.5 μm , with the cubic NaA crystals closely packed in the shell. Some small defeat holes can be observed in its higher resolution image (Fig. 1c insert). With the average size of NaA crystals of about 1.0 μm , the thin shell was composed of one-layer NaA

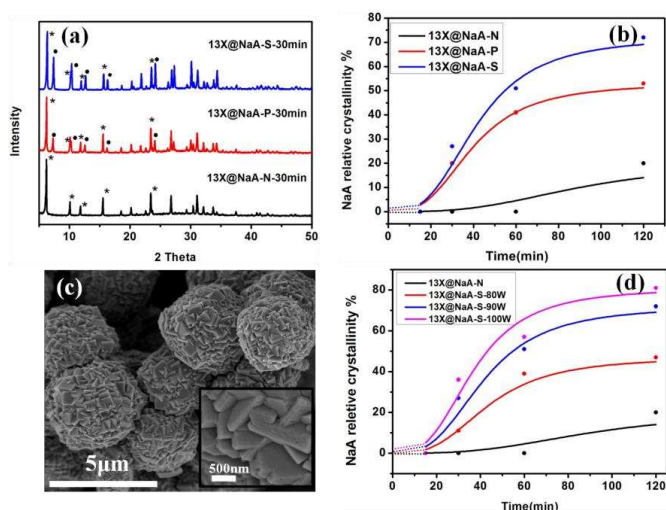


Fig 1 (a) XRD patterns of 13X@NaA-N/P/S after the crystallization aging for 60 min; where * denotes the characteristic peaks of 13X, and • denotes those of NaA; (b) the change of crystallinity of NaA in 13X@NaA-N/P/S with the aging time under the input power of 90 W; (c) SEM images of 13X@NaA-S-60; (d) the effect of input power of the plasma treatment on the crystallinity of 13X@NaA-S.

crystals. When the aging time was even shortened to 15 min (Fig. S2c), the characteristic peaks of NaA in all the samples disappeared. Therefore, with the crystallization aging time was shortened to about 30 min, the plasma treatment can effectively accelerate the formation rate of NaA crystal shell on the surface of 13X powders.

We further adjusted the input power of the plasma treatments to understand its acceleration effect on the formation of NaA shell. In the case of the plasma treatment for 13X powders (Fig. S4), the crystallinities of NaA in 13X@NaA-P under 90 W were all larger than those under 80 W at whatever aging times. However, increasing the strength of input power to 100 W, the crystallinities showed a little further enhancement. Whereas in the case of the plasma treatment for both 13X powders and the mixed precursor gel (Fig. 1d), when the aging time was 30 min, the almost liner accelerating effect of the input powder on the crystallinity of NaA shell suggested the plasma treatment can significantly increase the initial crystallization rate. The crystallinity of NaA was as high as 40% under 100 W. When prolonging the aging time, the acceleration effect on the crystallinity of NaA changed gently. At 120 min, the crystallinity of NaA in 13X@NaA-S-120 reached 81% and 72% under 100 W and 90 W input powers, respectively, much higher than that in 13X@NaA-N-120 produced by the normal crystallization method.

To clearly reveal the mechanism of the acceleration mechanism of the plasma treatment, the active reaction species of

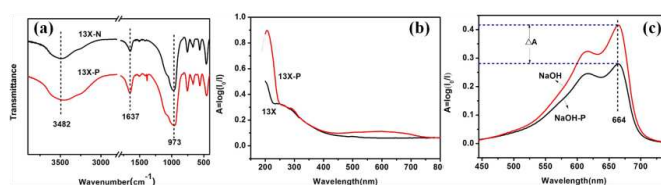


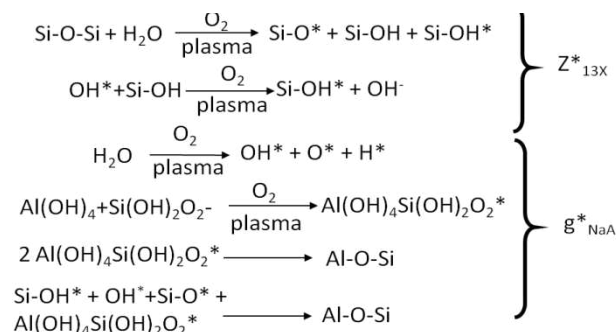
Fig 2 Characterization of the effects of plasma treatments (a) FTIR spectra of 13X and 13X-P, (b) UV spectra of 13X and 13X-P, (c) UV spectra of NaOH with MB scavenger.

the hydroxyl group on the surface of 13X-P powders and the free radicals generated in the mixed precursor gels were then determined, respectively. Compared 13X-P-90 sample with the pristine 13X, the FTIR spectra (Fig. 2a) showed similar characteristic bands at 973 cm^{-1} and 3482 cm^{-1} , which were assigned to the groups of Si-O-Si and -OH,²⁷ but their relative intensity ratios were significantly different. Accordingly, the larger integral area ratio of the -OH band to that of Si-O-Si ($R_{\text{OH/Si-O-Si}}$) revealed directly much more active -OH groups in 13X-P-90. However, since the -OH band at 3482 cm^{-1} is attributed to both contributions of Si-OH group and H₂O molecule, we had to carefully eliminate the influence of residual water in the samples. When we checked the band of H₂O at 1637 cm^{-1} , the integral area ratio of $R_{\text{H}_2\text{O/Si-O-Si}}$ of two samples of 13X and 13X-P were calculated as the same as 0.2, suggesting the residual water can be regarded as the same. Then after the calibration, $R_{\text{OH/Si-O-Si}}$ of 13X-P-90 was 0.9, apparently higher than 0.6 of 13X, confirming the amount of -OH groups on the surface of 13X-P-90 was significantly increased after the DBD plasma treatment under oxygen atmosphere.

In contrast to the UV spectrum (Fig. 2b) of 13X with almost no absorption in the whole wave range of 200–800 nm, the UV spectrum of 13X-P-90 exhibited a significant absorption peak at about 200 nm, attributed to the absorption of oxygen atom in the hydroxyl group. Therefore, the plasma treatment successfully produced more -OH groups on the surface of 13X-P-90. The amount of -OH groups produced by the plasma treatment was determined by the comparison of the TG curves of 13X-P-90 and 13X (Fig. S5). Both TG curves of 13X and 13X-P-90 showed a significant weight loss before 100°C, attributed to the adsorbed water and impurities. Since the difference of the weight loss between them was less than 1%, the residual water in 13X and 13X-P-90 samples can be considered almost the same after the pre-treatment. When increasing the temperature above 200°C, the weight loss attributed to the decomposition of surface -OH groups was much more significant for 13X-P-90 than 13X. The amount of -OH groups increased in 13X-P-90 after the plasma treatment was then determined as 4 wt.%.

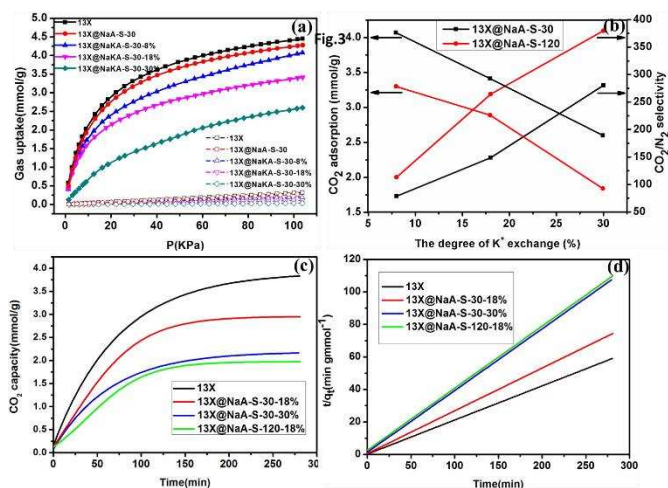
Meanwhile, the radicals produced in the mixed precursor gel through the plasma treatment was demonstrated by the methylene blue (MB) scavenger trapping test. As a good •OH radical scavenger, MB has a high affinity for the •OH radical through the sulfur atom, and changes into colorless hydroxylated methylene blue (MB-OH).²⁸ Because the silica gel-sol suspension is not suitable for the UV spectrophotometric detection, we simplified the mixed precursor gel into NaOH solution, which was the main resource media for producing free radicals after the plasma treatment.^{29,30} NaOH solution was treated with plasma at a relatively moderate power of 90W, the UV spectra of MB in NaOH solution after the plasma treatment showed a significant decrease of absorbance at 664 nm (Fig. 2c). Calculated from the change of absorbance, 33% MB were decomposed caused by the same amount of •OH free radicals produced by the plasma treatment.

Fig 3 (a) CO₂ and N₂ adsorption isotherms at 298 K on 13X@NaA-S-30 under different degrees of potassium ion exchanges, (b) trade-offs between CO₂ adsorption capacity and the selectivity $S_{\text{CO}_2/\text{N}_2}$ of 13X@NaA-S-120 and 13X@NaA-S-30 at 298 K and 1 bar, (c) dynamic CO₂ adsorption at 298 K of 13X and 13X@NaA-S-30/120 after potassium ion exchange, (d) fitting plots of t/q_t against t as predicted by the second-order rate law.



Scheme 1 Three detours to produce 13X@NaA-N/P/S composites and their acceleration mechanism through the plasma treatment.

As illustrated in Scheme 1, with three different detours to produce 13X@NaA-N/P/S composites, the formation rate of NaA can be generalized as $dZ_{\text{NaA}}/dt = kZ_{13X}^a Z_{13X}^*{}^b g_{\text{NaA}}^c g_{\text{NaA}}^*{}^d$, in which Z_{13X} and g_{NaA} are the concentrations of 13X and NaA precursor, Z_{13X}^* and g_{NaA}^* are their corresponding concentrations after the plasma treatments, a , b , c and d were their reaction orders. Comparing the changes of the relative crystallinity of NaA among 13X@NaA-N/P/S composites (Fig. 1b), both plasma treatments can accelerate the formation rate of NaA crystals on the surface of 13X powders, accordingly, Z_{13X}^* and g_{NaA}^* played more important roles in the formation of NaA. Although the double plasma treatments definitely improved the crystallinity of NaA, the improvement by the plasma treatment for the mixed precursor gel was not as significant as that for 13X powders, which inferred the contribution of Z_{13X}^* is larger than g_{NaA}^* for the formation of NaA. Therefore, the reaction



orders in the formation of 13X@NaA-S might be in the sequence of $b > d > a \approx c$. After the plasma treatments, the increased amount of -OH groups on the surface of 13X powders and the existence of •OH free radicals in mixed precursor gel resulted in the concentration

increases of Z_{13X}^* and g_{NaA}^* , respectively, and hence the formation rate of NaA crystal shell was significantly improved.

As we know, the commercial 13X zeolite is a good CO₂ adsorbent but shows relatively low selectivity. Based on the difference of kinetic radius between CO₂ (0.330 nm) and N₂ (0.364 nm), we adjusted the window size of NaA crystals in the thin shell of 13X@NaA composites through a potassium ion exchange.³¹⁻³⁴ With controlled pore size in the NaA shell, N₂ molecules can be dynamically blocked to enter the 13X core, and hence to improve the CO₂/N₂ selectivity. N₂ adsorption and desorption isotherms at 77 K of 13X@NaKA-S-30 composites revealed a decrease of surface area with increasing the degree of potassium ion exchange (Fig. S6). At high degree of potassium ion exchange, such as 30%, the surface area of 13X@NaKA-30 was as low as 30.9 m²·g⁻¹. As a result, both pure CO₂ and N₂ adsorption capacities at 298 K on 13X@NaKA-S-30 composites decreased with increasing the degree of potassium ion exchange (Fig. 3a). However, the decrease of N₂ adsorption capacity was even much significant due to the well-controlled pore size of NaKA in the thin shell (Table S1), accordingly, the higher selectivity S_{CO_2/N_2} was obtained. As shown in Fig. 3b, a trade-off between CO₂ adsorption capacity and the selectivity S_{CO_2/N_2} can be observed as the degree of potassium ion exchange changed. With 8.0 % potassium ion exchange, 13X@NaKA-S-30-8% showed a good CO₂ adsorption capacity of 4.07 mmol·g⁻¹ but a relatively lower S_{CO_2/N_2} of 78.6. When the potassium ion exchange was 18 %, S_{CO_2/N_2} was significantly enhanced to 148.8, with CO₂ adsorption capacity of 3.41 mmol·g⁻¹. After 30% potassium ion exchange, S_{CO_2/N_2} was even enhanced to 280.5, with the CO₂ adsorption capacity maintained at 2.60 mmol·g⁻¹. To gain deeper insight the influence of the NaA crystallinity and the thickness of the shell, 13X@NaA-S-120 was also selected as a comparison. With the corresponding similar potassium ion exchange, 13X@NaA-S-120 showed a similar trade-off trend but with relatively lower CO₂ adsorption capacity and higher selectivity (Fig. 3b, Fig. S7). For example, at 18% potassium ion exchange, with CO₂ adsorption capacity as 2.89 mmol·g⁻¹, S_{CO_2/N_2} was already as high as 264.4. The S_{CO_2/N_2} can be further increased to 379.7 when 30% potassium ion exchange, but a very low capacity due to the blockage of the skeleton pore of the shell by potassium ion. Therefore, with suitable potassium ion exchange in the thin NaKA shell, the S_{CO_2/N_2} can be significantly improved with good adsorption capacity maintained.

So far, due to the shrunk pore size in the shell, the effect of potassium ion exchange on the adsorption rate also aroused our great concerns. To demonstrate the CO₂ dynamic adsorption performance more accurately, instead of the adsorption from pure gas, the gas mixture (15% CO₂ and 85% N₂) was used to simulate the flue gas. The second-order kinetic model (Eq. 3) was used to fitting the dynamic adsorption data.

$$\frac{t}{q_t} = \frac{1}{kq_e^2} + \frac{1}{q_e}t \quad (3)$$

where q_e and q_t (mmol·g⁻¹) are the CO₂ adsorption uptakes at saturated and at any time t , respectively; k (g·mmol⁻¹·min⁻¹) is the rate constant of a second-order kinetics model. Compared with the pristine 13X, the CO₂ uptakes of 13X@NaKA-S-30/120 samples unavoidably decreased (Fig. 3c); and it decreased even more with

increasing the degree of potassium ion exchange and the aging time. For all the samples, good linear relationships of plottings of (t/q_t) against t with the correlation coefficient R very close to 1 were obtained (Fig. 3d), suggesting the second-order adsorption kinetics can describe the adsorption performance well. As listed in Table S2, the values of k (g·mmol⁻¹·min⁻¹) and q_e (mmol·g⁻¹) decreased in the following order: pristine 13X (0.35, 3.83) > 13X@NaKA-S-30-18% (0.22, 2.95) > 13X@NaKA-S-30-30% (0.16, 2.16) > 13X@NaKA-S-120-18% (0.10, 1.97). Both the adsorption rate and capacity of 13X@NaKA-S-30-18% were quite acceptable, however, some deviation in CO₂ uptake indicated that the dynamics involved in the gas separation was more complex than based on thermodynamic effects alone. The correlation can be ascribed to the relation between CO₂ diffusion rate and the rate at which the system will approach the equilibrium. Accordingly, the total CO₂ uptake can then be estimated by combining the equilibrium uptakes with the correction factor of the root relative diffusion constant D_s^{rel} as Eq. 4³⁵

$$q_{tot} = \sqrt{D_s^{rel}} q_e, \quad D_s^{rel} = D_s/D_{s0} \quad (4)$$

where D_{s0} refers to the CO₂ self-diffusion coefficient in zeolite NaA, and D_s is that after the potassium ion exchange. For 13X@NaKA-S-30-30% and 13X@NaKA-S-120-18%, with more degree of potassium ion exchange and longer aging time, more serious blockage and thicker shell resulted in the lower CO₂ diffusion constant D_s , in turn, the adsorption rate and saturated uptakes. Therefore, take account for the real extent of freedom that the gas molecules have to diffuse and reach to adsorption equilibrium, 13X@NaKA-S-30-18% was the optimized CO₂ adsorbent, combining the high adsorption capacity, selectivity and rate.

Compared with those reported zeolite-based materials (the CO₂ capacity and S_{CO_2/N_2}) which showed good CO₂ adsorption performance (Table S3), like NaK-ZK-4 (2.50 mmol/g at 293 K; 880 at 273K),³⁴ Cu-SSZ-13 (3.75 mmol/g, 72.0) and H-SSZ-13 (3.98mmol/g, 73.6),³⁶ the samples in this work, like 13X@NaKA-S-30-18% (3.41mmol/g, 148.8), showed both good CO₂ capacity and high selectivity. The most noteworthy is that the synthesis of reported zeolite-based materials were generally based on the traditional thermal crystallization route, which were quite time-consuming and usually needed expensive structure template reagent. With the plasma treatment, without any structure template reagent, the synthesis time of 30 min in this work was greatly reduced. Moreover, the side-effect of potassium ion exchange was the significant decline of the adsorption rate,³⁴ especially for a whole particle with specific sizes. It is our understanding that the core@shell structure with potassium ion exchange in the thin shell would be a guarantee for both good equilibrium and dynamic CO₂ adsorption performance. Whereas for those state-of-the-art materials with excellent CO₂ adsorption performance, such as the porous organic polymers (POPs),³⁷⁻⁴¹ metal organic frameworks (MOFs)⁴²⁻⁴⁴ and covalent organic frameworks (COFs),^{45,46} as listed in Table S3, usually showed a trade-off between the CO₂ capacity and selectivity. Moreover, as

POPs or MOFs not only needed a long-time synthesis, but also usually had very complex multistep procedures involving costly organometallic catalysts, which needed great endeavours in specific monomers or ligands designing and fabrication, therefore, their practical applications in real carbon capture remained great challenges.

Conclusions

In summary, an ultra-fast synthesis of core-shell 13X@NaA composites through the DBD plasma treatment under O₂ atmosphere was realized. With the plasma treatments, more silanol hydroxyl groups were produced uniformly on the surface 13X powders and hydroxyl free radicals were induced in the NaA precursor gel, which effectively accelerated the formation of dense NaA crystal shell on the surface of 13X powders. Only after 30 min aging, 13X@NaA-S-30 composite with a thin uniform NaA crystal shell can be obtained. The window size of NaA crystals was effectively adjusted by the potassium ion exchange to hinder the entrance of N₂ molecules, and hence the CO₂ adsorption selectivity was significantly improved. Among them, 13X@NaKA-S-30 with 18 % potassium ion exchange showed both excellent equilibrium and dynamic CO₂ adsorption performance, with the ideal selectivity of CO₂ over N₂ of 172.6, CO₂ capacity of 3.41 mmol·g⁻¹, and adsorption rate constant of 0.22 g·mmol⁻¹·min⁻¹ from the simulated flue gas. This approach not only enables us to achieve an excellent CO₂ capture adsorbent, but also provides promising methods for synthesis of core-shell zeolite composites as economic materials for further multiple applications.

Acknowledgment

Financial support for this work is provided by the National Basic Research Program of China (2015BAC04B01), the National Natural Science Foundation of China (No. 91334203, 21376074, 21676080), the project of FP7-PEOPLE-2013-IRSES (PIRSSES-GA-2013-612230), Shanghai Municipal Bureau of Quality and Technical Supervision Foundation of China (No. 2015-03)

Notes and references

- 1 F. Su, C. Lu, S. C. Kuo and W. Zeng, *Energy and Fuels.*, 2010, **24**, 1441–1448.
- 2 S. K. Wirawan and D. Creaser, *Microporous Mesoporous Mater.*, 2006, **91**, 196–205.
- 3 G. D. Pirngruber, C. Laroche, M. Maricar-Pichon, L. Rouleau, Y. Bouizi and V. Valtchev, *Microporous Mesoporous Mater.*, 2013, **169**, 212–217.
- 4 X. Wang, S. Guo and L. Zhao, *Bull. Korean Chem. Soc.*, 2013, **34**, 3829–3834.
- 5 R. H. P. R. Poladi and C. C. Landry, *J. Solid State Chem.*, 2002, **167**, 363–369.
- 6 L. Huang, W. Guo, P. Deng, Z. Xue and Q. Li, *J. Phys. Chem. B.*, 2000, **104**, 2817–2823.
- 7 Q. Zhang, C. Li, S. Xu, H. Shan and C. Yang, *J. Porous Mater.*, 2013, **20**, 171–176.
- 8 S. P. ZHDANOV, *Adv. Chem.*, 1974, **2**, 20–43.
- 9 Z. Zhou, G. Jin, H. Liu, J. Wu and J. Mei, *Appl. Clay Sci.*, 2014, **97–98**, 110–114.
- 10 M. Severance, B. Wang, K. Ramasubramanian, L. Zhao, W. S. W. Ho and P. K. Dutta, *Langmuir*, 2014, **30**, 6929–6937.
- 11 M. B. Park, N. H. Ahn, R. W. Broach, C. P. Nicholas, G. J. Lewis and S. B. Hong, *Chem. Mater.*, 2015, **27**, 1574–1582.
- 12 C. Belviso, F. Cavalcante and S. Fiore, *Ultrason. Sonochem.*, 2013, **20**, 32–36.
- 13 S. H. Jhung, T. Jin, Y. K. Hwang and J. S. Chang, *Chem. - A Eur. J.*, 2007, **13**, 4410–4417.
- 14 G. Feng, P. Cheng, W. Yan, M. Boronat, X. Li, J.-H. Su, J. Wang, Y. Li, A. Corma, R. Xu and J. Yu, *Science.*, 2016, **351**, 1188–91.
- 15 H. Yasuda, *Polym. Prepr. (Am. Chem. Soc., Div. Polym. Chem.)*, 1975, **16**, 57–59.
- 16 J. P. Boudou, J. I. Paredes, A. Cuesta, A. Martínez-Alonso and J. M. D. Tascón, *Carbon.*, 2003, **41**, 41–56.
- 17 P. Chu, *Mater. Sci. Eng. R.*, 2002, **36**, 143–206.
- 18 C. Oehr, *Nucl. Instr. and Meth. in Phys. Res. B.*, 2003, **208**, 40–47.
- 19 E. M. Liston, L. Martinu and M. R. Wertheimer, *J. Adhes. Sci. Technol.*, 1993, **7**, 1091–1127.
- 20 S. Guruvenket, G. M. Rao, M. Komath and A. M. Raichur, *Appl. Surf. Sci.*, 2004, **236**, 278–284.
- 21 C. J. Liu, K. Yu, Y. P. Zhang, X. Zhu, F. He and B. Eliasson, *Appl. Catal. B Environ.*, 2004, **47**, 95–100.
- 22 H. Ming and K. M. Spark, *J. Phys. Chem. B*, 2003, **107**, 694–702.
- 23 J. Gao, X. Zhu, Z. Bian, T. Jin, J. Hu and H. Liu, *Microporous Mesoporous Mater.*, 2015, **202**, 16–21.
- 24 J. Gao, J. Xu, S. Wen, J. Hu and H. Liu, *Microporous Mesoporous Mater.*, 2015, **207**, 149–155.
- 25 M. Hudis, *J. Appl. Polym. Sci.*, 1972, **16**, 2397–2415.
- 26 J. I. E. R. Chen, *J. Appl. Polym. Sci.*, 1991, **42**, 2035–2037.
- 27 M. Ide, M. El-Roz, E. De Canck, A. Vicente, T. Planckaert, T. Bogaerts, I. Van Driessche, F. Lynen, V. Van Speybroeck, F. Thybault-Starzyk and P. Van Der Voort, *Phys. Chem. Chem. Phys.*, 2012, **15**, 642–650.
- 28 A. Y. Satoh, J. E. Trosko and S. J. Masten, *Environ. Sci. Technol.*, 2007, **41**, 2881–2887.
- 29 A. Tani, Y. Ono, S. Fukui, S. Ikawa and K. Kitano, *Appl. Phys. Lett.*, 2012, **100**, 2012–2015.
- 30 T. Takamatsu, K. Uehara, Y. Sasaki, H. Miyahara, Y. Matsumura, A. Iwasawa, N. Ito, T. Azuma, M. Kohno and A. Okino, *RSC Adv.*, 2014, **4**, 39901–39905.
- 31 D. W. Breck, W. G. Eversole, R. M. Milton, T. B. Reed and T. L. Thomas, *J. Am. Chem. Soc.*, 1956, **78**, 5963–5972.
- 32 Q. Liu, A. Mace, Z. Bacsik, J. Sun, A. Laaksonen and N. Hedin, *Chem. Commun.*, 2010, **46**, 4502–4504.
- 33 F. Akhtar, Q. Liu, N. Hedin, L. Bergstrom, *Energy Environ. Sci.*, 2012, **5**, 7664–7673.
- 34 O. Cheung, Z. Bacsik, P. Krokidas, A. Mace, Aa. Laaksonen, and N. Hedin, *Langmuir.*, 2014, **30**, 9682–9690.
- 35 A. Mace, N. Hedin and A. Laaksonen, *J. Phys. Chem. C.*, 2013, **117**, 24259–24267.
- 36 M. R. Hudson, W. L. Queen, J. A. Mason, D. W. Fickel, R. F. Lobo and C. M. Brown, *J. Am. Chem. Soc.*, 2012, **134**, 1970–1973.
- 37 H. A. Patel, H. Je, J. Park, Y. Jung and A. Coskun, *Chem. Eur. J.*, 2014, **20**, 772 – 780.
- 38 H. A. Patel, S. H. Je, J. Park, D. P. Chen, Y. Jung, C. T. Yavuz and A. Coskun, *Nat. Commun.*, 2013, **4**, 1357–1358.
- 39 M. Saleh, S. Bin Baek, H. M. Lee and K. S. Kim, *J. Phys. Chem. C.*, 2015, **119**, 5395–5402.
- 40 F. Jiang, T. Jin, X. Zhu, Z. Tian, J. Hu, D. Jiang, H. Wang, H. Liu and S. Dai, *Macromolecules.*, 2016, **49**, 5325–5330.
- 41 Y. Zhu, H. Long and W. Zhang, *Chem. Mater.*, 2013, **25**, 1630–1635.
- 42 S. Bao, R. Krishna, Y. He, J. Qin, Z. Su, S. Li, W. Xie, D. Du, W. He, S. Zhang and Y. Lan, *J. Mater. Chem. A.*, 2015, **3**, 7361–7367.
- 43 A. Banerjee, S. Nandi and P. Nasa, *Chem. Commun.*, 2016, **52**, 1851–1854.

- 44 J. Li, J. Yu, W. Lu, L. Sun, J. Sculley and P. B. Balbuena, *Nat. Commun.*, 2013, **4**, 1538.
- 45 R. Ge, D. Hao, Q. Shi, B. Dong, W. Leng, C. Wang and Y. Gao, *J. Chem. Eng. Data*, 2016, **61**, 1904–1909.
- 46 G. Lin, H. Ding, D. Yuan, B. Wang and C. Wang, *J. Am. Chem. Soc.* 2016, **138**, 3302–3305.